J. Appl. Comput. Mech., 7(1) (2021) 148-164
DOI: 10.22055/JACM.2020.34699.2460

ISSN: 2383-4536
jacm.scu.ac.ir

Shahid Chamran University of Ahvaz

Journal of Applied and Computational Mechanics

Research Paper

Nonlinear Winkler-based Frame Element with Inclusion of Shear-Flexure Interaction Effect for Analysis of Non-Ductile RC Members on Foundation

Worathep Sae-Long[1], Suchart Limkatanyu[2], Pattamad Panedpojaman[3], Woraphot Prachasaree[4], Nattapong Damrongwiriyanupap[5], Minho Kwon[6], Chayanon Hansapinyo[7]

[1] Civil Engineering Program, School of Engineering, University of Phayao, Phayao, 56000, Thailand, Email: worathep.sa@up.ac.th

[2] Department of Civil Engineering, Faculty of Engineering, Prince of Songkla University, Songkhla, 90112, Thailand, Email: suchart.l@ psu.ac.th

[3] Department of Civil Engineering, Faculty of Engineering, Prince of Songkla University, Songkhla, 90112, Thailand, Email: ppattamad@eng.psu.ac.th

[4] Department of Civil Engineering, Faculty of Engineering, Prince of Songkla University, Songkhla, 90112, Thailand, Email: woraphot.p@psu.ac.th

[5] Civil Engineering Program, School of Engineering, University of Phayao, Phayao, 56000, Thailand, Email: nattapong.da@up.ac.th

[6] Department of Civil Engineering, ERI, Gyeongsang National University, Jinju, 660-701, South Korea, Email: kwonm@gnu.ac.kr

[7] Center of Excellence in Natural Disaster Management, Department of Civil Engineering, Chiang Mai University, Chiang Mai, 50200, Thailand, Email: chayanon@eng.cmu.ac.th

Received August 20 2020; Revised September 23 2020; Accepted for publication September 23 2020.
Corresponding author: Worathep Sae-Long (worathep.sa@up.ac.th)

Abstract. Non-ductile reinforced concrete (RC) members are common in the existing RC frame buildings with the old seismic code (lightly and inadequately detailed transverse reinforcement) and may suffer shear failure or flexure-shear failure. To investigate the failure behaviors of those RC structures, performance-based numerical models are needed. Thus, a new fiber frame element on Winkler-based foundation including the interaction effects between shear and flexure was developed to analyze non-ductile RC frames resting on foundation, in this study. The proposed element is formulated for implementation in displacement-based finite element formulation under the kinematic assumptions of Timoshenko beam theory. As a result, axial and flexural mechanisms are automatically coupled through the fiber-section model, while shear and flexural actions interact via the UCSD shear-strength model within the framework of modified Mergos-Kappos interaction procedure to evaluate sectional shear force and shear stiffness within the shear constitutive law. Therefore, the presented model is simple, but able to capture several salient behaviors of non-ductile RC frames resting on foundation, including interaction between shear and flexure, soil-structure interaction, degradation of shear strength due to inelastic flexural deformation, and shear failure. Those features and efficiency of the proposed model are demonstrated by two numerical simulations in this work.

Keywords: RC frame element, Soil-structure interaction, Shear-flexure interaction, Winkler foundation, Flexure-shear critical column.

1. Introduction

The problem of soil-structure interaction has gotten attention and has been studied extensively in the structural and geotechnical engineering community for several decades. This problem relates to several engineering tasks, for example, highway pavement [1-2], structure foundation members [3-6], geotechnical structures [7], etc. Therefore, understanding sophisticated behaviors of structural members on foundation plays an essential role in realistic modeling for design of those types of structures. Furthermore, it is also a challenging problem to development of performance-based numerical models in the structural engineering field.

Nowadays, there is a large variety of numerical models with various approaches to represent soil-structure interaction within structural models. From the excellent literature reviews Dutta and Roy [8] and Menglin et al. [9], there are two general concepts to represent mechanical behavior of the foundation medium. The first one is the continuous model [10]. These models can give comprehensive details on variation of force and deformation within the foundation medium. However, this model type is limited to engineering problems when the solution of the partial differential equations is needed. Furthermore, unreasonable predictions of foundation displacement outside the loaded region have been demonstrated with these models [11]. The second one is the subgrade model [12]. These models are the favorite type in structural engineering as they avoid the boundary problems in sophisticated solution of partial differential equations in the continuous model. However, as an alternative the Winkler foundation model [13] has been widely employed. It represents behaviors of the foundation medium by a series of discrete

Published online: September 24 2020

springs instead of a single value with the subgrade modulus. Thus, the Winkler foundation model is often called the "one-parameter" foundation model.

To apply the Winkler foundation model within the structural models, it is well-known that there are two classical beam theories to describe the kinematic assumptions of the structures, namely Euler-Bernoulli beam theory and Timoshenko beam theory [14]. In the different kinematic assumptions of these theories, the plane section after deformation is normal to the reference beam axis for the Euler-Bernoulli beam theory, while the plane section based on the Timoshenko beam theory is not normal to the reference beam axis due to shear effect. Therefore, the kinematic assumption in Timoshenko beam theory is more suitable than the Euler-Bernoulli beam theory for the analysis of structural members with a small span-to-depth ratio (shear dominant characteristic). In the past decades, a large number of numerical models for the analysis of Timoshenko beam-columns on foundation have been proposed. For example, Cheng and Pantelides [15] presented a dynamic matrix for the Timoshenko beam-column elements on elastic foundation, for dynamic analysis, and later extended this to cover the elastic two-parameter foundation by Monsalve et al. [16]. Yokoyama [17] presented the matrix equation based on Hamilton's principle to study vibration behaviors of Timoshenko beam-columns on elastic two-parameter foundation. Taha and Abdeen [18] proposed an analytical solution of the Timoshenko beam-column resting on a two-parameter foundation by using a recursive differentiation approach (considering the angular inertia and shear stress induced by the axial load). However, although these models are accurate and efficient for the static and dynamic analysis of the Timoshenko beam-column on foundation, natural characteristics of material constitutive models for the analysis of reinforced concrete (RC) members are not taken into account within these models. Furthermore, the behaviors of the foundation are not only limited to within the elastic range.

For the analysis of a non-ductile RC beam-column on the foundation, not only must we require suitable material models, but also have to consider the influence of shear effect within the analytical model. It is well-known that RC beam-column with a low span-to-depth ratio will suffer a shear failure or flexure-shear failure, especially the RC beam-columns with old seismic code (insufficient design of the transverse reinforcements).

Consideration of the shear mechanism within the structural models is also more complicated than flexure action. Furthermore, the degree of complexity in this problem drastically increases when the inelastic flexure deformation affects the shear resistance capacity, as observed in several experimental tests of non-ductile RC columns [19-24]. This phenomenon is defined as the "shear-flexure" interaction, which is always found in the flexure-shear critical RC members (failed in shear after flexural yielding).

There are several strategies to include the interaction effect between shear and flexure within the fiber structure models, as excellently concluded in the research work of Ceresa et al. [25]. For example, a series of multi-dimensional concrete models have been employed to couple flexure and shear within the fiber structure element at the material and section level [26-30]. Although this approach is very accurate and can represent several concrete features, the procedure to evaluate the sectional force and sectional stiffness within the material constitutive models is more complicated. An alternative way to include the coupling effect between shear and flexure within the fiber structure element is a series of flexure springs and/or shear springs at the end of the structure element. Marini and Spacone [31] used the force-based formulation to couple the shear and flexure of their Timoshenko fiber frame element through equilibrium enforcement at the element level. However, the shear strength based on Eurocode 2 [32] was underestimated due to no consideration of the aspect ratio. Mergos and Kappos [33] presented the gradual spread inelastic beam-column based on the sub-element of Soleimani [34]. The interaction between shear and flexure in their model was presented within the sectional state determination of the shear hysteretic law, modified from the proposals of Ozcebe and Saatcioglu [35]. It included the concrete cracking, the flexure yielding (plastic-hinge formation), and the onset of transverse reinforcement yielding. Later, the shear model of Mergos and Koppos [33] was improved to capture the failure characteristics of non-ductile columns (e.g. shear failure [36] and axial loss capacity [37]). Xu and Zhang [38] modified the hysteretic shear model of Ozcebe and Saatcioglu [35] to couple the shear and flexural mechanisms. The interaction between shear and flexure of this model did not only couple at the section level through the primary curve but also at the element level by enforcing local and global equilibria during the hysteretic procedure. However, this model did not include axial load effect. Sea-Long et al. [39, 40] extended the shear hysteretic model of Mergos and Kappos [33, 36] to non-ductile RC column under cyclic loading. The superiority of this model when compared to other above discussed models was the natural prediction of the plastic-hinge formation based on the fiber-section model, a pinching effect, the degradation of shear strength due to the inelastic flexural deformation, and the stiffness degradation with increasing displacement. However, the model of Sea-Long et al. [39, 40] does not cover the analysis of non-ductile RC member on foundation.

In light of the limitations to capture sophisticated behaviors of non-ductile RC members resting on foundation, as above discussed in relation to several previous models, the development of a fiber frame element on foundation was well motivated. This study presents a new fiber frame element resting on Winkler-based foundation, taking into account the coupling of shear and flexure action for static analysis of the non-ductile RC member resting on foundation. To the best knowledge of the authors, this is the first presentation of a fiber RC frame model resting on Winkler-based foundation with inclusion of interaction between shear and flexural action. The proposed element is formulated within the framework of displacement-based formulation, under the kinematic assumptions of Timoshenko beam theory. The nonlinear nature of the proposed model is in the constitutive laws for each material (including the nonlinear nature of the foundation).

The sequence of presentation in this paper starts from the governing differential equations. It includes the sectional equilibrium, sectional compatibility, and force-deformation relations at the fiber-section level. Then, the displacement-based formulation is employed to formulate the stiffness of the proposed element. The general implementation of both the strong and the weak forms of the proposed element are conveniently presented by the modified Tonti diagram [41]. Next, the sectional shear force-shear strain relation is introduced. It includes the primary undamaged curve, damaged curve with shear-flexure interaction based on the UCSD (University of California, San Diego) shear-strength model [20], and modified procedure to predict the sectional shear stiffness and shear force [39, 40]. Finally, the capability and performance of the proposed element to capture several features of a non-ductile RC member on nonlinear foundation are validated through two numerical simulations. All of the numerical simulations with the proposed element in this paper were implemented on the general-purpose finite element platform FEAP [42].

2. A Series of Differential Equation for Timoshenko Frame on Winkler-Based Foundation

2.1 System Equilibrium

The frame resting on the foundation subjected to the external transverse load $p_y(x)$ along the frame length as shown in Figure 1 (a) is the typical model to represent the behaviors of non-ductile RC frame on the foundation in this work. The internal equilibrium equations of this frame system are obtained by considering the free body diagram of an infinitesimal segment dx

under the small deformation assumption as shown in Figure 1 (b). The equilibrium equations in the longitudinal axis, rotation axis, and transverse axis yield the following relations:

$$\frac{dN_f(x)}{dx} = 0 \tag{1}$$

$$\frac{dM_f(x)}{dx} + V_f(x) = 0 \tag{2}$$

$$\frac{dV_f(x)}{dx} + p_y(x) - D_s(x) = 0 \tag{3}$$

where $N_f(x)$, $M_f(x)$, and $V_f(x)$ represent the sectional axial force, bending moment, and shear force in the frame element, respectively; and $D_s(x)$ is the foundation interactive force.

Eqs. (1) to (3) represent the governing differential equilibrium equations of the Timoshenko frame resting on Winkler-based foundation and can be grouped into matrix form for a simplified symbolic formula:

$$\mathbf{L}_{TF}^T \mathbf{D}_{TF}(x) + \mathbf{L}_F^T \mathbf{D}_F(x) - \mathbf{p}(x) = \mathbf{0} \tag{4}$$

in which

$$\begin{aligned} \mathbf{D}_{TF}(x) &= \left\{ N_f(x) \quad M_f(x) \quad V_f(x) \right\}^T \\ \mathbf{D}_F(x) &= \left\{ D_s(x) \right\}^T \\ \mathbf{p}(x) &= \left\{ 0 \quad 0 \quad p_y(x) \right\}^T \end{aligned} \tag{5}$$

and $\mathbf{D}_{TF}(x)$, $\mathbf{D}_F(x)$, and $\mathbf{p}(x)$ are the vectors containing the Timoshenko frame sectional forces, the foundation interactive force, and the external distributed loads, respectively. The differential operators $\mathbf{L}_{TF}$ and $\mathbf{L}_F$ are expressed as follows:

$$\mathbf{L}_{TF} = \begin{bmatrix} \frac{d}{dx} & 0 & 0 \\ 0 & \frac{d}{dx} & 0 \\ 0 & 1 & -\frac{d}{dx} \end{bmatrix} \text{ and } \mathbf{L}_F = \begin{bmatrix} 0 & 0 & 1 \end{bmatrix} \tag{6}$$

Following the equilibrium equations of eqs. (1) to (3), it is observed that there are four internal force unknowns, while only three equilibrium equations are available to determine these internal forces. Thus, this frame system in this study can be considered an internally statically indeterminate system. However, this is not a principal problem for displacement-based elements when the sectional forces can be evaluated from the approximated sectional displacement fields through the compatibility relations and the sectional constitutive laws, respectively.

2.2 Compatibility Relations

The relations between the element deformations and element displacements at any section of frame and foundation are expressed through the compatibility conditions. The Timoshenko frame deformation vector $\mathbf{d}_{TF}(x)$ is the conjugate work pair of the Timoshenko frame force vector $\mathbf{D}_{TF}(x)$ and is defined as:

$$\mathbf{d}_{TF}(x) = \left\{ \varepsilon_f(x) \quad \kappa_f(x) \quad \gamma_f(x) \right\}^T \tag{7}$$

where $\varepsilon_f(x)$, $\kappa_f(x)$, and $\gamma_f(x)$ are, respectively, the sectional axial strain, bending curvature, and shear strain of the frame element. Similarly, the sectional displacement fields are grouped into the displacement vector $\mathbf{u}(x)$, which is expressed as:

$$\mathbf{u}(x) = \left\{ u_x(x) \quad \theta(x) \quad u_y(x) \right\}^T \tag{8}$$

where $u_x(x)$ and $u_y(x)$ are, respectively, the axial and transverse displacement at any section on the reference axis; and $\theta(x)$ is the sectional rotation.

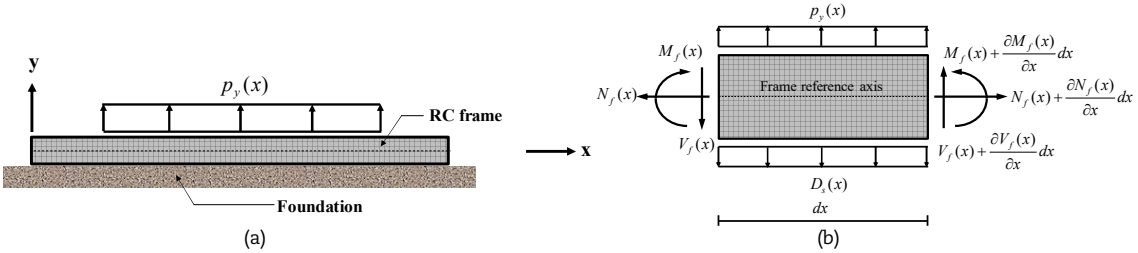

Fig. 1. Timoshenko frame resting on foundation: (a) Typical system; and (b) Free body diagram of infinitesimal segment *dx*.

Based on the fundamental hypothesis of Timoshenko beam theory [14] that "*Plane section remains plane but loses normality to the longitudinal beam axis due to shear deformation*", the deformation-displacement relations of the frame model in the Cartesian coordinate system can be expressed as follows [43]:

$$\varepsilon_f(x) = \frac{du_x(x)}{dx} \tag{9}$$

$$\kappa_f(x) = \frac{d\theta(x)}{dx} \tag{10}$$

$$\gamma_f(x) = \theta(x) - \frac{du_y(x)}{dx} \tag{11}$$

The compatibility conditions of frame element in eqs. (9) to (11) can be written in vector form as:

$$\mathbf{d}_{TF}(x) = \mathbf{L}_{TF}\mathbf{u}(x) \tag{12}$$

The foundation deformation vector $\mathbf{d}_F(x)$ is the conjugate work pair of the foundation force vector $\mathbf{D}_F(x)$ and is defined as:

$$\mathbf{d}_F(x) = \{0 \quad 0 \quad \Delta_s(x)\}^T \tag{13}$$

where $\Delta_s(x)$ is the sectional foundation deformation. Based on the fundamental kinematic assumption of the Winkler foundation model [44], the foundation deformation $\Delta_s(x)$ is assumed to be perfectly compatible with the transverse displacement of RC frame $u_y(x)$. Thus, the relation between the foundation deformation $\Delta_s(x)$ and the transverse displacement $u_y(x)$ can be written as:

$$\Delta_s(x) = u_y(x) \tag{14}$$

Following the differential operator $\mathbf{L}_F$ of eq. (6), the foundation deformation vector $\mathbf{d}_F(x)$ of eq. (13), and the compatibility relation of eq. (14), the foundation deformation vector $\mathbf{d}_F(x)$ can be rewritten as:

$$\mathbf{d}_F(x) = \mathbf{L}_F\mathbf{u}(x) \tag{15}$$

It is noteworthy to point out that the system equilibrium of eq. (4) and system compatibility of eqs. (12) and (15) relate through the differential operators $\mathbf{L}_{TF}$ and $\mathbf{L}_F$. This observation relies on the fact that the frame system in the current work is contragradient.

2.3 Force-Deformation Relations

The nonlinear nature of the proposed model in this study emerges from the nonlinear force-deformation relations, which depends on each material models. Thus, the sectional force of Timoshenko frame $\mathbf{D}_{TF}(x)$ and foundation $\mathbf{D}_F(x)$ can be written as functions of sectional deformation:

$$\mathbf{D}_{TF}(x) = \Psi[\mathbf{d}_{TF}(x)] \text{ and } \mathbf{D}_F(x) = \Xi[\mathbf{d}_F(x)] \tag{16}$$

The incremental form of the nonlinear force-deformation relations in eq. (16) is obtained by linearization:

$$\begin{aligned} \mathbf{D}_{TF}(x) &= \mathbf{D}^0_{TF}(x) + \mathbf{k}^0_{TF}(x)\Delta\mathbf{d}_{TF}(x) \\ \mathbf{D}_F(x) &= \mathbf{D}^0_F(x) + \mathbf{k}^0_F(x)\Delta\mathbf{d}_F(x) \end{aligned} \tag{17}$$

where $\mathbf{D}^0_{TF}(x)$ and $\mathbf{D}^0_F(x)$ are the Timoshenko frame and foundation sectional force vectors, while $\mathbf{k}^0_{TF}(x)$ and $\mathbf{k}^0_F(x)$ are the stiffness matrices of Timoshenko frame and foundation, respectively. A superscript 0 on the symbols indicates the initial point of a vector or a matrix for iterative steps that follow.

In order to refine the element cross-section mesh for capturing inelastic flexural characteristics, the fiber-section model [45] is used to subdivide the frame cross-section into discrete fibers (layers) as shown in Figure 2. Following this approach, the axial and flexural mechanisms are automatically coupled. Thus, the axial force $N_f(x)$ and moment $M_f(x)$ at any section are obtained as sum of normal stress and the geometric properties at each fiber, as follows:

$$N_f(x) = \sum_{p=1}^{nfib} \sigma_p A_p \text{ and } M_f(x) = -\sum_{p=1}^{nfib} y_p \sigma_p A_p \tag{18}$$

where σ_p, A_p and y_p are the normal stress, the area, and the distance from the reference axis x, respectively, of the p^{th} fiber in the section; *p* indicates the generic fiber; and *nfib* represents the number of fibers in the section.

Following the sectional axial force and bending moment discretization of eq. (18), the Timoshenko frame sectional force vector $\mathbf{D}_{TF}(x)$ of eq. (5) can be rewritten as:

$$\mathbf{D}_{TF}(x)=\left\{\sum_{p=1}^{nfib}\sigma_p A_p \quad -\sum_{p=1}^{nfib}y_p\sigma_p A_p \quad V(x)\right\}^T \tag{19}$$

It is salient to note that in the Timoshenko frame sectional force vector $\mathbf{D}_{TF}(x)$ of eq. (19) the axial and flexural actions depend on the variation of the normal stress σ_p along the section depth via the section discretization of the fiber-section model, while the shear action is a constant force along the section depth via Timoshenko beam theory [43]. Thus, only one-fiber discretization is sufficient for the shear action in any section.

Based on the fiber-section model, the Timoshenko frame sectional stiffness matrix $\mathbf{k}_{TF}(x)$ and the foundation sectional stiffness matrix $\mathbf{k}_F(x)$ can be defined as:

$$\mathbf{k}_{TF}(x)=\begin{bmatrix}\sum_{p=1}^{nfib}E_pA_p & -\sum_{p=1}^{nfib}y_pE_pA_p & 0\\ -\sum_{p=1}^{nfib}y_pE_pA_p & \sum_{p=1}^{nfib}y_p{}^2E_pA_p & 0\\ 0 & 0 & GA_s(x)\end{bmatrix} \text{ and } \mathbf{k}_F(x)=\left[k_s(x)\right] \tag{20}$$

where E_p is the modulus of the p^{th} fiber in the section; $GA_s(x)$ is the sectional shear stiffness; and $k_s(x)$ is the sectional foundation stiffness. The Timoshenko frame sectional stiffness matrix $\mathbf{k}_{TF}(x)$ of eq. (20) demonstrates that shear action does not couple with the axial and flexural mechanisms directly. However, the shear and flexural actions are related through the "*UCSD Shear-Strength Model*" [20] within the framework of the modified Mergos and Kappos shear-flexure interaction procedure [39] and will be discussed later.

To describe the material behaviors of RC frame on Winkler-based foundation, this study uses the uniaxial constitutive laws to represent the behaviors of each model implementation. The concrete is represented by the Kent and Park model [46]; the reinforcing steel bars are represented by the Menegotto and Pinto model [47]; the bi-linear force-deformation is used for the Winkler foundation springs [44]; and the modified Mergos and Kappos model [39] is employed for shear response. All primary constitutive laws of each material models are shown in Figure 3.

From the governing equations of the Timoshenko frame model on Winkler-based foundation, the equilibrium, compatibility, and force-deformation equations as discussed above can be conveniently presented in the classical Tonti's diagram in Figure 4 (a). This diagram will be adopted to present the weak state of governing equations within the framework of the displacement-based formulation in the next section.

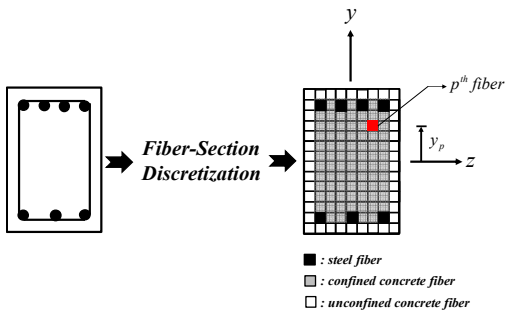

Fig. 2. Fiber discretization of RC frame cross-section [45].

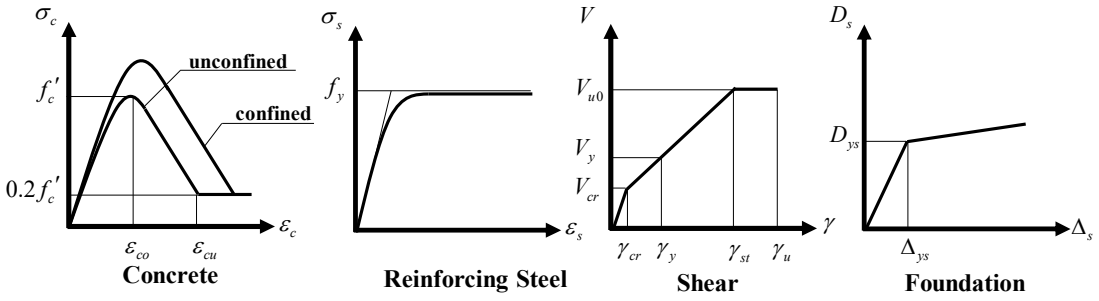

Fig. 3. Uniaxial constitutive laws [39].

3. The Weak State of Timoshenko Frame on Winkler-Based Foundation (The Principle of Virtual Displacement)

3.1 Formulation

Following the procedure of displacement-based finite element formulation, the element nodal displacements $\mathbf{U}$ serve as the primary variables. The sectional displacements $\mathbf{u}(x)$ can be evaluated from the element nodal displacements $\mathbf{U}$ through the displacement shape functions. Then the sectional deformations $\mathbf{d}_{TF}(x)$ and $\mathbf{d}_{F}(x)$ can be determined from the sectional displacements $\mathbf{u}(x)$ by enforcing the compatibility conditions in eqs. (12) and (15). As a result, the compatibility relations at the section level are satisfied point-by-point along the element length while the equilibrium equation in eq. (4) is satisfied in the integral sense through the principle of virtual displacement. All of the above discussion can be summarized in the modified Tonti's diagram in Figure 4 (b).

The weighted residual form of equilibrium equation in eq. (4) can be written as:

$$\int_L \delta\mathbf{u}^T(x)\left[\mathbf{L}_{TF}^T\mathbf{D}_{TF}(x)+\mathbf{L}_F^T\mathbf{D}_F(x)-\mathbf{p}(x)=\mathbf{0}\right]dx=0 \tag{21}$$

where $\delta\mathbf{u}(x)$ is the statically admissible virtual section displacement vector.

Imposing the linearized force-deformation relations of eq. (17) into (21) and enforcing compatibility of eqs. (12) and (15) leads to:

$$\int_L \delta\mathbf{u}^T(x)\begin{bmatrix}\mathbf{L}_{TF}^T\left(\mathbf{D}_{TF}^0(x)+\mathbf{k}_{TF}^0(x)\mathbf{L}_{TF}\Delta\mathbf{u}(x)\right)+\\ \mathbf{L}_F^T\left(\mathbf{D}_F^0(x)+\mathbf{k}_F^0(x)\mathbf{L}_F\Delta\mathbf{u}(x)\right)-\mathbf{p}(x)\end{bmatrix}dx=0 \tag{22}$$

To transfer the order of the differential operators $\mathbf{L}_{TF}$ and $\mathbf{L}_F$ from the section force vectors $\mathbf{D}_{TF}(x)$ and $\mathbf{D}_F(x)$ into the virtual sectional displacement $\delta\mathbf{u}(x)$, integration by parts is applied to eq. (22):

$$\begin{aligned}&\int_L\left(\mathbf{L}_{TF}\delta\mathbf{u}\ (x)\right)^T\mathbf{k}_{TF}^0(x)\left(\mathbf{L}_{TF}\Delta\mathbf{u}(x)\right)dx+\int_L\left(\mathbf{L}_F\delta\mathbf{u}\ (x)\right)^T\mathbf{k}_F^0(x)\left(\mathbf{L}_F\Delta\mathbf{u}(x)\right)dx\\&=\delta\mathbf{U}^T\mathbf{P}+\int_L\delta\mathbf{u}^T(x)\mathbf{p}(x)dx-\int_L\left(\mathbf{L}_{TF}\delta\mathbf{u}\ (x)\right)^T\mathbf{D}_{TF}^0(x)dx-\int_L\left(\mathbf{L}_F\delta\mathbf{u}\ (x)\right)^T\mathbf{D}_F^0(x)dx\end{aligned} \tag{23}$$

where $\delta\mathbf{U}^T\mathbf{P}$ represent the boundary terms from integration by parts. Furthermore, $\delta\mathbf{U}^T\mathbf{P}$ denotes the external virtual work done by the applied nodal forces $\mathbf{P}$ on the virtual nodal displacements $\mathbf{U}$.

Following the displacement-based formulation, the displacement fields $\mathbf{u}(x)$ can be evaluated from the element nodal displacements $\mathbf{U}$ through the displacement shape function matrix $\mathbf{N}_L(x)$ as:

$$\mathbf{u}(x)=\mathbf{N}_L(x)\mathbf{U} \tag{24}$$

The displacement shape functions $\mathbf{N}_L(x)$ in eq. (24) for the Timoshenko frame element should selected with care, because they can suffer to a problematic phenomenon of "*shear locking*" that leads to unrealistic displacement responses in slender members, as discussed in detail by Onate [43]. This study avoids this problem by using so-called "*linked*" displacement shape functions [48] to evaluate the sectional displacements $\mathbf{u}(x)$. This kind of displacement interpolation functions is made from the sectional transverse displacement $u_y(x)$ with a quadratic (bubble) term. As a result, the sectional transverse displacement $u_y(x)$ is one-degree higher than the sectional rotation field $\theta(x)$ and the bubble term can be expressed in terms of the nodal rotations (U_3 and U_6) through the limitation of the slender beams ($\gamma_f=0$). More details on the linked displacement shape functions are given by Sae-Long et al. [39]. The linked displacement shape functions are:

$$u_x(x)=\left(1-\frac{x}{L}\right)U_1+\frac{x}{L}U_4 \tag{25}$$

$$\theta(x)=\left(1-\frac{x}{L}\right)U_3+\frac{x}{L}U_6 \tag{26}$$

$$u_y(x)=\left(1-\frac{x}{L}\right)U_2+\frac{x}{L}U_5+\left(\frac{x}{2}-\frac{x^2}{2L}\right)U_3+\left(-\frac{x}{2}+\frac{x^2}{2L}\right)U_6 \tag{27}$$

where U_1, U_2, U_3, U_4, U_5, and U_6 are the element nodal displacements, which are contained in the element nodal displacements vector $\mathbf{U}$. Following the eqs. (25) to (27), the displacement shape functions $\mathbf{N}_L(x)$ are given by Sae-Long et al. [39] as:

$$\mathbf{N}_L(x)=\begin{bmatrix}1-\frac{x}{L} & 0 & 0 & \frac{x}{L} & 0 & 0\\ 0 & 0 & 1-\frac{x}{L} & 0 & 0 & \frac{x}{L}\\ 0 & 1-\frac{x}{L} & \frac{x}{2}-\frac{x^2}{2L} & 0 & \frac{x}{L} & -\frac{x}{2}+\frac{x^2}{2L}\end{bmatrix} \tag{28}$$

Substituting eq. (24) into (23) and considering the arbitrariness of $\delta\mathbf{U}$ leads to:

$$\left[\int_L \mathbf{B}_{TF}(x)^T \mathbf{k}_{TF}^0(x)\mathbf{B}_{TF}(x)dx + \int_L \mathbf{N}_F(x)^T \mathbf{k}_F^0(x)\mathbf{N}_F(x)dx\right]\Delta\mathbf{U} = \mathbf{P} + \int_L \mathbf{N}_L(x)^T \mathbf{p}(x)dx - \int_L \mathbf{B}_{TF}(x)^T \mathbf{D}_{TF}^0(x)dx - \int_L \mathbf{N}_F(x)^T \mathbf{D}_F^0(x)dx \tag{29}$$

where $\mathbf{B}_{TF}(x)$ and $\mathbf{N}_F(x)$ are the sectional deformation-displacement matrices given by:

$$\mathbf{B}_{TF}(x) = \mathbf{L}_{TF}\mathbf{N}_L(x) = \begin{bmatrix} -\frac{1}{L} & 0 & 0 & \frac{1}{L} & 0 & 0 \\ 0 & 0 & -\frac{1}{L} & 0 & 0 & \frac{1}{L} \\ 0 & \frac{1}{L} & \frac{1}{2} & 0 & -\frac{1}{L} & \frac{1}{2} \end{bmatrix} \text{ and } \mathbf{N}_F(x) = \mathbf{L}_F\mathbf{N}_L(x) = \begin{bmatrix} 0 & 0 & 0 & 0 & 0 & 0 \\ 0 & 0 & 0 & 0 & 0 & 0 \\ 0 & 1-\frac{x}{L} & \frac{x}{2}-\frac{x^2}{2L} & 0 & \frac{x}{L} & -\frac{x}{2}+\frac{x^2}{2L} \end{bmatrix} \tag{30}$$

The expression of eq. (29) can be written in the element stiffness equation as:

$$\left(\mathbf{K}_{TF}^0 + \mathbf{K}_F^0\right)\Delta\mathbf{U} = \left(\mathbf{P} + \mathbf{P}_P\right) - \mathbf{P}_{TF}^0 - \mathbf{P}_F^0 \tag{31}$$

where $\mathbf{K}_{TF}^0 = \int_L \mathbf{B}_{TF}(x)^T \mathbf{k}_{TF}^0(x)\mathbf{B}_{TF}(x)dx$ and $\mathbf{K}_F^0 = \int_L \mathbf{N}_F(x)^T \mathbf{k}_F^0(x)\mathbf{N}_F(x)dx$ are, respectively, the Timoshenko frame and foundation element stiffness matrices; $\mathbf{P}_{TF}^0 = \int_L \mathbf{B}_{TF}(x)^T \mathbf{D}_{TF}^0(x)dx$ and $\mathbf{P}_F^0 = \int_L \mathbf{N}_F(x)^T \mathbf{D}_F^0(x)dx$ are, respectively, the Timoshenko frame and foundation element resisting force vectors; and $\mathbf{P}_P = \int_L \mathbf{N}_L(x)^T \mathbf{p}(x)dx$ is the equivalent load vector due to the distributed load $\mathbf{p}(x)$.

It is noted that the incremental form of the element stiffness equation in eq. (31) is the core of the displacement-based finite formulation for the Timoshenko frame element resting on the Winkler-based foundation, as shown in Figure 5. The term on the right-hand-side in eq. (31) represents the residual force vector corresponding to the equilibrium equations, which are weakened by the principle of virtual displacement. The residual force vector will vanish when the equilibrium configuration is reached during the incremental-iterative solution procedure.

4. Sectional Shear Force – Deformation Relation

4.1 Undamaged Primary Curve

To describe the relationship between shear force and shear strain at the section level, this study starts from the undamaged primary curve illustrated in Figure 6. This diagram has four parts but only three different slopes to represent the behaviors of the RC members. The original diagram was first proposed by Mergos and Kappos [33] and later modified by Mergos and Kappos [36], Zimos et al. [37], and Sae-Long et al. [39, 40]. However, the root of development in this shear diagram by these researchers is similar. For this study, the shear constitutive law developed by the authors [39] is used to represent the shear response. It can be briefly explained as follows.

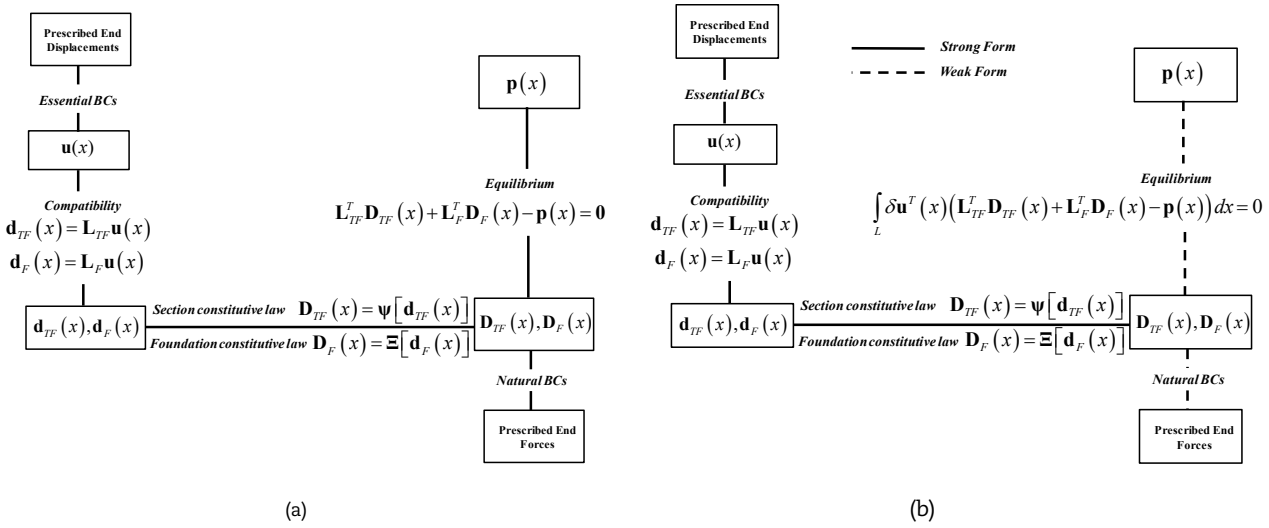

Fig. 4. Tonti's diagram of RC frame model on Winkler foundation: (a) Strong form; and (b) Weak form [41].

The first part shows the uncracked behavior of reinforced concrete: shear response with the linear segment OA corresponding to the uncraked slope $(GA)_0$. The origin point O towards to the cracking point A (V_{cr}, γ_{cr}) at which the nominal principal tensile stress is higher than the nominal tensile strength of concrete. The cracking shear force V_{cr}, the uncracked shear slope $(GA)_0$, and the cracking shear strain γ_{cr} are calculated from the equations introduced by Sezen and Moehle [49]:

$$\begin{aligned} V_{cr} &= \left(\frac{f_t^{'}}{(L_a / h)} \sqrt{\left(1 + \frac{N}{f_t^{'} A_g}\right)} \right) 0.80 A_g \\ (GA)_0 &= 0.80 G A_g \\ \gamma_{cr} &= \frac{V_{cr}}{(GA)_0} \end{aligned} \tag{32}$$

where $f_t^{'}$ represent the nominal tensile strength of concrete; L_a / h defines to the shear span ratio; A_g is the gross cross sectional area and G is the concrete shear modulus.

The second part presents the behavior of reinforced concrete after cracked formation with the linear segment AB. The cracked concrete at point A (V_{cr}, γ_{cr}) connects to the flexural yielding at point B (V_y, γ_y) with a slope $(GA)_1$. Based on the fiber-section model, the yielding shear force V_y and shear strain γ_y are kept updated when the axial strain in longitudinal reinforcement reaches yielding strain for the first time.

Similarly, the third part has the same slope as the second part $(GA)_1$ in the linear segment BC but this part represents the behavior of reinforced concrete after the plastic hinge. The flexural-yielding point B (V_y, γ_y) links to the point C (V_{u0}, γ_{st}) at which the shear force reaches its ultimate value V_{u0} while the shear strain experiences onset of transverse reinforcement yielding γ_{st}. To evaluate the ultimate value of the shear strength, this study employs the so-called "*UCSD Shear-Strength Model*" proposed by Priestley et al. [20] to capture the behavior of the shear strength deterioration with increasing curvature ductility demand. The name of this shear strength model refers to the University of California, San Diego (UCSD). The UCSD shear-strength V_u is given by:

$$V_u = k_\varphi \sqrt{f_c'} \left(0.8 A_g\right) + \frac{A_v f_{yv} D'}{s} \cot 30^0 + N \tan \beta \tag{33}$$

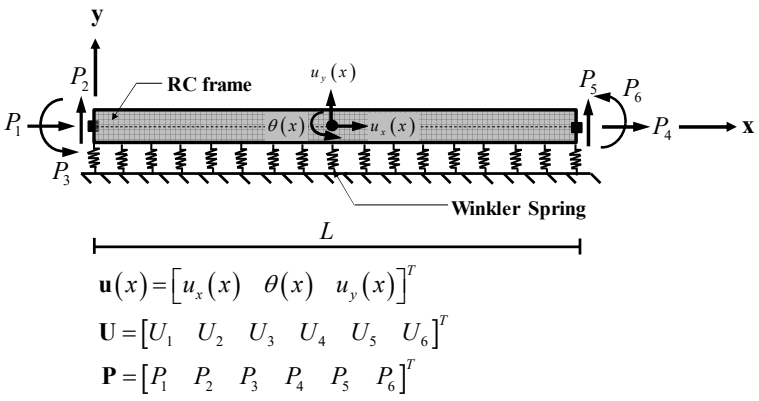

Fig. 5. RC frame element on Winkler foundation system.

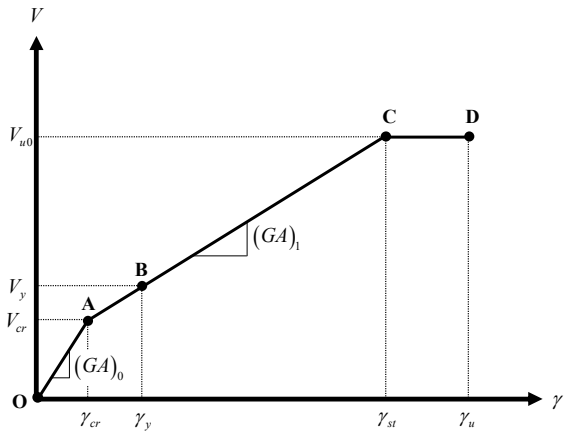

Fig. 6. Undamaged primary curve of sectional shear constitutive law [36].

where k_φ is a reduction parameter due to the influence of sectional curvature ductility, μ_φ on the shear strength in the concrete component as shown in Figure 7; f_c' is the concrete strength; A_g, s, and f_{yv} are, respectively, the area, spacing, and yield strength of transverse reinforcement; D' is the distance measured parallel to the applied shear between centers of the longitudinal reinforcement; N is the axial load (compression); and β is the angle between the column axis and the line connecting the centers of the flexural compression zones at the top and the bottom of the column ends.

The shear strain at the onset of transverse reinforcement yielding γ_{st} can simply be determined from the truss analogy [50]. However, the shear strain γ_{st} based on the truss analogy did not match experimental results well. Later, Mergos and Kappos [33, 36] improved this approach by multiplication with two modification factors from regression analysis. The first factor κ considers the axial-load effect while the second factor λ includes the member-aspect ratio effect. Thus, the shear strain γ_{st} is given by

$$\gamma_{st} = \kappa \lambda \gamma_{truss} \tag{34}$$

where $\kappa = 1 - 1.07(N / f_c' A_g)$ is the modification factor associated with axial-force; $\lambda = 5.37 - 1.59 \min(2.5, L_a / h)$ is the modification factor associated with aspect ratio; and γ_{truss} is the shear strain based on the truss analogy approach [50] corresponding to transverse reinforcement yielding. This leads to the following expression:

$$\gamma_{truss} = \frac{V_{cr}}{(GA)_0} + \frac{A_v f_{yv}}{s E_s b \rho_w \sin^4 \omega \cot \omega}\left(\sin^4 \omega + \frac{E_s}{E_c}\rho_w\right) \tag{35}$$

where E_s and E_c are, respectively, the elastic modulus of steel and concrete; ρ_w is the volumetric ratio of transverse reinforcement; b is the width of cross section; and ω is the angle between frame reference axis and the line of diagonal struts. The optimal value of angle ω in this study follows the research work of Mergos and Kappos [36] that defined its value about 45°. This value is accepted based on experimental and analytical results.

Finally, the last part with flat-top linear CD on the primary curve represents plastic shear response. This part connects the shear-yielding point C (V_{u0}, γ_{st}) to the ultimate point D (V_{u0}, γ_u) at which the shear strain reaches shear strain at the onset of shear failure γ_u. The behavior of shear response on the last part is obtained from the experimental observation that shear strain of the shear-critical reinforced concrete members can increase after the yielding point of transverse reinforcement until onset of shear failure [36, 51-54]. Thus, the value of the shear strain γ_u can become higher than the shear strain γ_{st}. The equation to predict the shear strain γ_u is given by Mergos and Kappos [36] who employed twenty-five shear and flexure-shear critical RC columns in regression analyses to propose the shear strain at the onset of shear failure γ_u as:

$$\gamma_u = \lambda_1 \lambda_2 \lambda_3 \gamma_{st} \geq \gamma_{st} \tag{36}$$

The shear strain γ_u is estimated from the shear strain γ_{st} with three modified parameters: the parameter considering axial load $\lambda_1 = 1 - 2.5 \min(0.4, N / f_c' A_g)$; the parameter accounting for the member aspect ratio $\lambda_2 = \min(6.25, L_a^2 / h^2)$; and the parameter associated with amount of transverse reinforcement $\lambda_3 = 0.31 + 17.8 \min(A_v f_{yv} / b s f_c', 0.08)$.

4.2 Procedure of Shear-Flexure Interaction

The influence of the interaction between shear and flexural mechanisms on the column responses has long been recognized in the research community. The previous research works [19, 20, 23, 55] demonstrated that the inelastic flexural deformation influences shear resistance. In other words, the shear strength of the RC members in the plastic hinge region decreases with inelastic flexural deformation. The degradation of shear strength is caused by damage to concrete associated with the inelastic flexural deformation (Plastic-hinge formation). Moreover, several experimental results [22, 23] indicate that the sectional shear strain in the plastic hinge region increases drastically following the inelastic flexural deformation while the shear force is constant. Both phenomena are caused by the influences of the shear-flexure interaction effects. In order to include both results in the finite element analysis, Mergos and Kappos [33, 36] introduced the interaction procedure that combines the UCSD shear-strength model [20] and the truss analogy approach [50] in the analysis of non-ductile RC columns.

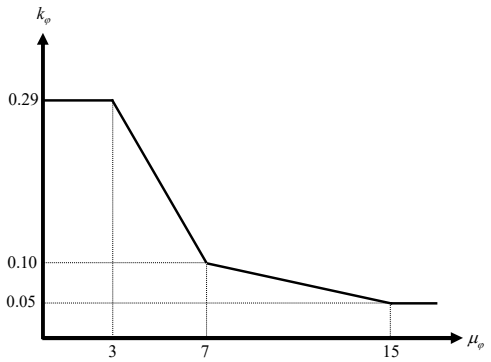

Fig. 7. The relation between reduced factor k_φ and curvature ductility μ_φ [36].

In the current study, the shear-flexure interaction procedure introduced by Sae-Long et al. [39] is used. Figure 8 presents the general scheme for the interaction between shear and flexure and the development of the degraded shear envelope curve with increasing curvature ductility demand μ_φ. The reduced shear strength associated with the degradation of the concrete shear-strength component V_c, as defined by the UCSD shear-strength model in eq. (33) influences the undamaged shear envelope curve. In other words, the sectional shear response starts to deviate from the undamaged envelope curve when there is shear strength degradation. The damaged (reduced) envelope curve is updated with the evolution of the degraded shear strength and the resulting envelope curve is along the path $O-A-B-E-F'-G'-H'-C^G-D^G$ as shown in Figure 8.

The shear-flexure interaction process of Sea-Long et al. [39] was originally presented by Mergos and Kappos [36]. The procedure is established from the geometric relation between the shear force increment ΔV and shear strain increment $\Delta\gamma$ at section level to determine the shear force increment ΔV and the effective shear stiffness $(GA)_{eff}$ at any section. Therefore, this process is called the "*modified Mergos-Kappos*" shear-flexure interaction procedure [39].

In the so-called "*modified Mergos-Kappos*" shear-flexure interaction procedure, the reference shear stiffness $(GA_{ref})_i^k$ is established between the undamaged state and the analytical state. It can be defined as:

$$\left(GA_{ref}\right)_i^k = \frac{V_{0,i}^{k+1} - V^k}{\Delta\gamma_i^k} \tag{37}$$

where $V_{0,i}^{k+1} = V_{cr} + (GA)_1(\gamma_i^{k+1} - \gamma_{cr})$ is the non-degraded sectional shear force corresponding to the sectional shear strain $\gamma_i^{k+1} = \gamma^k + \Delta\gamma_i^k$. From considering the geometric relation between the shear force increment ΔV_i^k and shear strain increment $\Delta\gamma_i^k$, it can be written as follows:

$$\Delta\gamma_i^k = \frac{\Delta V_i^k}{\left(GA_{eff}\right)_i^k} = \frac{\Delta V_i^k + \left(\Delta V_c^{deg}\right)_i^k}{\left(GA_{ref}\right)_i^k} \tag{38}$$

where $(\Delta V_c^{deg})_i^k$ is the reduced shear force corresponding to the shear strength degradation in the concrete based on the UCSD shear-strength model [20]. It can be determined as:

$$\left(\Delta V_c^{deg}\right)_i^k = \left(GA_{ref}\right)_i^k \Delta\gamma_i^k - \left(\frac{V_{ui}^k - V^k}{\gamma_{st} - \gamma^k}\right)\Delta\gamma_i^k \tag{39}$$

where V_{ui}^k is the degraded shear strength depending on variation of the concrete resisting shear force with the sectional curvature ductility μ_φ through a coefficient k_φ.

The effective sectional shear stiffness $(GA_{eff})_i^k$ is obtained by solving eq. (38) in terms of the reference sectional shear stiffness $(GA_{ref})_i^k$ as:

$$\left(GA_{eff}\right)_i^k = \frac{\Delta V_i^k}{\Delta V_i^k + \left(\Delta V_c^{deg}\right)_i^k}\left(GA_{ref}\right)_i^k \tag{40}$$

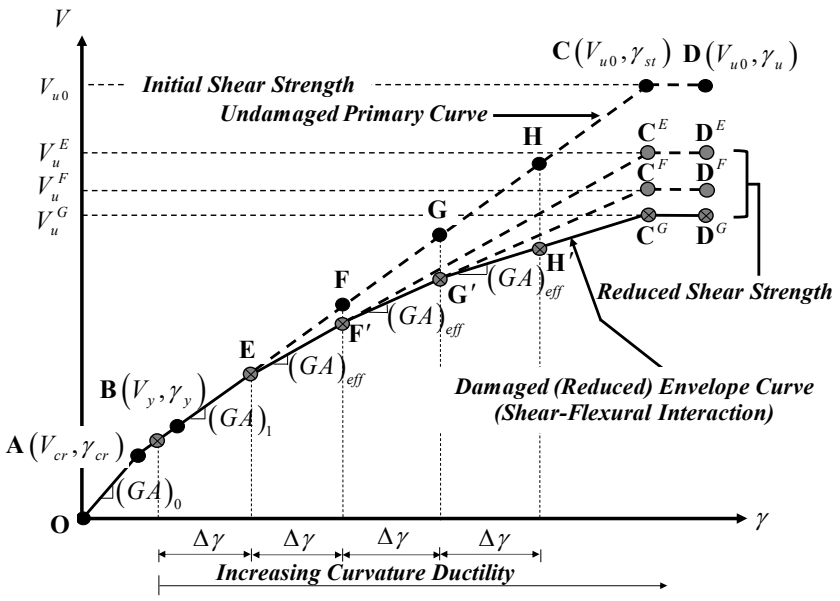

Fig. 8. Damaged envelope curve of sectional shear constitutive law [39].

However, it is noted that the shear force increment ΔV_i^k and the effective shear stiffness $(GA_{eff})_i^k$ at any section in eqs. (38) and (40) are unknown and mutually dependent. To determine both values, an additional iterative procedure with in the element iterative step i of the load increment k is proposed within the modified Mergos-Kappos shear-flexure interaction procedure. Furthermore, the variables $(GA_{ref})_i^k$, $(\Delta V_c^{deg})_i^k$, and $\Delta\gamma_i^k$ are not changed during this additional iterative process. A subscript index " j " is added into the variable ΔV_i^k and $(GA_{eff})_i^k$ to define the iterative step within the shear-flexure interaction procedure.

The residual function $\Phi((GA_{eff})_{i,j}^k)$ can be defined from the eqs. (38) and (40) as:

$$\Phi\left(\left(GA_{eff}\right)_{i,j}^k\right)=\left(GA_{eff}\right)_{i,j}^k\Delta\gamma_i^k-\frac{\left(GA_{eff}\right)_{i,j}^k\left(\Delta V_c^{deg}\right)_i^k}{\left(GA_{ref}\right)_i^k-\left(GA_{eff}\right)_{i,j}^k} \tag{41}$$

The Newton-Raphson method [56] is used to solve eq. (40). Thus, the derivative of eq. (41) by the effective shear stiffness $(GA_{eff})_{i,j}^k$ at any section is expressed as:

$$\frac{d\Phi\left(\left(GA_{eff}\right)_{i,j}^k\right)}{d\left(GA_{eff}\right)_{i,j}^k}=\Delta\gamma_i^k-\frac{\left(\Delta V_c^{deg}\right)_i^k}{\left(GA_{ref}\right)_i^k-\left(GA_{eff}\right)_{i,j}^k}-\frac{\left(GA_{eff}\right)_{i,j}^k\left(\Delta V_c^{deg}\right)_i^k}{\left(\left(GA_{ref}\right)_i^k-\left(GA_{eff}\right)_{i,j}^k\right)^2} \tag{42}$$

The step-by-step algorithm to determine the effective shear stiffness $(GA_{eff})_{i,j}^k$ and the current shear force V_i^{k+1} at any section within the shear-flexure interaction procedure is shown in Figure 9 and is fully described by Sae-Long et al. [39].

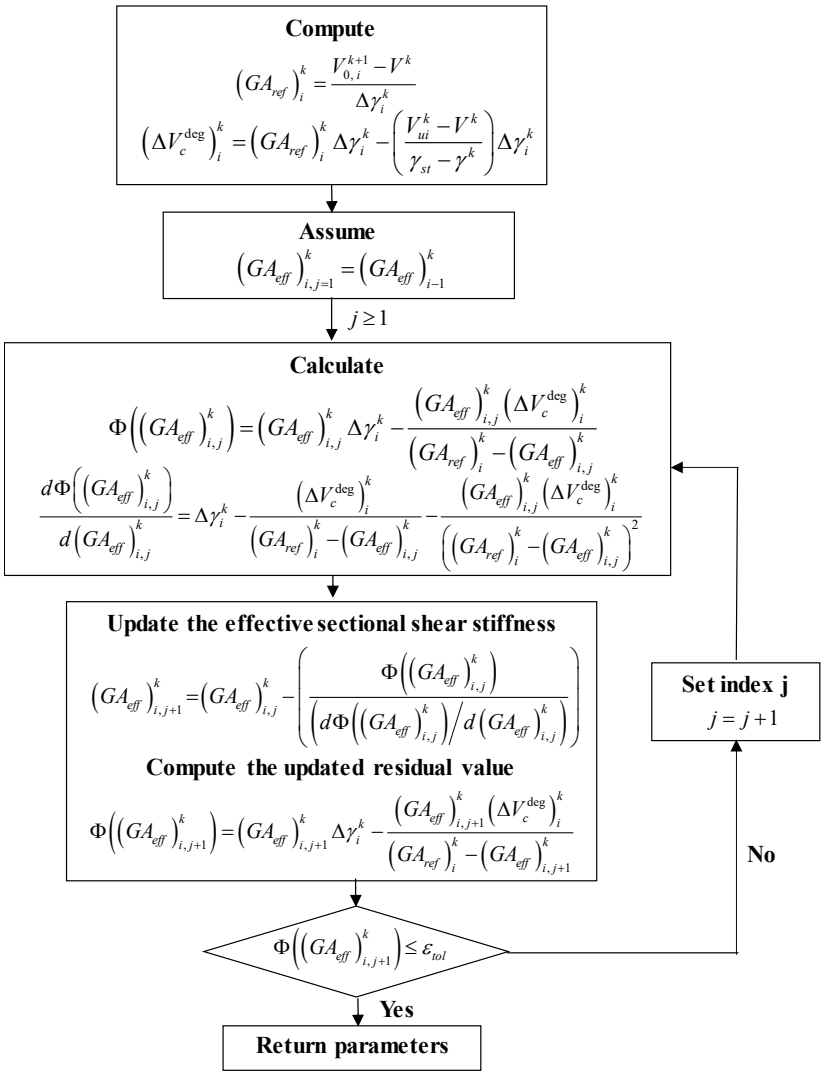

Fig. 9. The iterative process within the shear-flexure interaction procedure [39].

5. Numerical Simulations

To evaluate the performance, capabilities, and efficiency of the presented RC frame model on the foundation, two numerical simulations are provided in this paper. In the simulations of this study, the RC frame is selected from members that failed in shear following the flexural yielding. This kind of member is of so-called "*flexure-shear*" critical member type [57]. In the first simulation, both global and local convergence are assessed for the simply supported RC frame on nonlinear foundation, while the second simulation demonstrates the importance of considering shear-flexural interaction for analysis of flexure-shear critical RC member on foundation. Moreover, the effects of the foundation on the shear response are discussed in the second simulation.

5.1 Simulation I: Convergence Studies

In the first simulation, the simply supported RC frame resting on the foundation is subjected to midspan deflection under displacement-control and the constant compressive load at its tips of 667 kN as illustrated in Figure 10. This case is employed to study the convergence, performance, and efficiency of the proposed model. The geometry, material properties, and reinforcement detail of the RC frame as shown in Figure 10, obtained from one tested RC square columns representing older existing columns with light and insufficiently detailed transverse reinforcement [23]. The column labeled 2CLD12 was selected for use in this simulation. The characteristics of the foundation medium are: elastic-perfectly plastic with the initial stiffness k_s of 20 MPa and the foundation interactive force at the yielding point D_{ys} of 60 kN/m. Those properties of the foundation medium are based on simulation of the beam model on a two-parameter foundation proposed by Sapountzakis and Kampitsis [58]. Due to the symmetry of the model in this simulation, only half of the RC frame on the foundation is considered as shown in Figure 10. The analytical responses in this simulation are presented using seven Gauss-Lobatto integration points per element and the discretized frame cross-section with forty fibers (layers).

Figure 11 (a) presents an examination of the numbers of proposed elements required to obtain converged global response at the midspan deflection of 10 mm. The so-called "*benchmark*" response in this diagram is obtained from the response by using 16 of the proposed elements. It can be seen in this diagram that 8 proposed elements are sufficient to match the benchmark response in the global level. This number of elements is sufficient to get the converged solution. The response does not change even if the number of used elements increases. Furthermore, it can be observed in this plot that there are two changed slopes due to the yielding of foundation spring following the plastic hinge rotation in the RC frame. From the benchmark response, the yielding of foundation spring is detected at the midspan deflection of 3.1 mm while the first plastic hinge in the RC frame is detected at the midspan deflection of 5.7 mm. Finally, the shear failure is detected at the midspan deflection of 10.0 mm.

Figure 11 (b) shows the relation between shear force and shear strain (local response) at the midspan deflection of 10.0 mm obtained by using varied numbers of the proposed elements. The numbers of proposed elements to represent the benchmark response in this diagram was doubled from 16 to 32. Due to the restrain and load conditions, the plastic hinge is activated at the midspan of the RC frame. From the results of the benchmark, the proposed model predicts the sectional shear strain at the first plastic-hinge formation at about $\gamma_y = 8.1x10^{-4}$ corresponding to the midspan deflection of 5.7 mm. Next, the sectional curvature ductility is increased due to the increase of the applied deflection until it exceeds 3. The shear response starts to change from the undamaged primary curve to the damaged envelope curve due to the shear-flexure interaction as governed by the UCSD shear-strength model within the framework of the modified Mergos and Kappos shear-flexure interaction procedure. The shear stiffness and shear force are reduced and depend on the increase of the sectional curvature ductility demand. As a result, the shear strain significantly increased until shear failure was detected, at which point the shear strain at the ultimate state was about $\gamma_u = 12x10^{-3}$ corresponding to a midspan deflection of 10.0 mm.

To capture the behavior of the sectional curvature within the plastic hinge region, the number of proposed elements must give a more refined mesh. It can be observed from Figure 11 (b) that although 2, 4, and 8 of the proposed elements can closely predict the maximum shear force when compared to the benchmark response in the local level, these numbers of elements cannot capture the shear failure due to the lack of the accuracy in curvature ductility demand within the plastic hinge region. Thus, it is not a surprise that 16 elements can detect the shear failure and can represent the converged response in the benchmark with a sufficiently fined mesh to predict the sectional curvature ductility demand within the plastic hinge region.

5.2 Simulation II: The Effect of Shear-Flexure Interaction and the Influence of Foundation on The RC Frame Responses

The second simulation was run to reveal the effects of shear-flexure interaction and the influence of foundation on the responses of non-ductile RC frame. One RC square column tested by Lynn [22], namely the 2CMH18 column, was selected for simulation of a simply supported RC frame on elastic-perfectly plastic foundation subjected to a constant axial load of 1,512 kN at its tips and midspan deflection under displacement-control, as shown in Figure 12. The geometry, the details of reinforcement, and the material properties of this RC frame in Figure 12 come from the research work of Lynn [22] and those used by the authors to simulate the non-ductile RC frame element under cyclic loading [39]. The foundation force-deformation relation is assumed to be elastic-perfectly plastic. The properties of the foundation spring are similar to the previous simulation. In order to demonstrate the effect of shear-flexure interaction and the influence of the foundation on the responses of RC frame, there are three alternative analytical models used in comparisons, namely: (a) *the proposed frame model on foundation*; (b) *the classical Timoshenko frame model on foundation*, and (c) *the classical Timoshenko frame model*. It is noted that the so-called "*classical*" model is the model that does not take into account the shear-flexure interaction within the analytical model. All analytical responses in this simulation obtained from these models are presented with 16 elements having 7 Gauss-Lobatto integration points per element and the discretized frame cross-section with forty fibers (layers).

The midspan load-displacement (global response) as obtained from three different analytical models is shown in Figure 13. As observed from this plot, the responses by the proposed model and by the classical frame model on the foundation were almost identical, but slightly different in the final displacement-load step due to the shear-flexure interaction effect. There are three events in the global response: Point A with the foundation yielding point; Point B with the first plastic hinge formation; and Point C with the detected shear failure in the proposed model. The foundation yielding state at point A and the first plastic hinge formation at point B of both analytical models are similar and are detected at the midspan deflections 2.7 mm and 4.8 mm, respectively. However, the proposed model can detect the shear failure at point C when the sectional shear strain reaches the onset of shear failure $\gamma_u = 4.6x10^{-3}$ corresponding to the midspan deflection of about 9.6 mm. On the other hand, the classical Timoshenko frame model on the foundation cannot capture this behavior due to the lack of consideration of the shear-flexure interaction effect within the model implementation. Furthermore, this plot reveals that the element stiffness and shear resisting force increased due to the influence of the foundation medium, resulting in different points of the first plastic hinge formation between the models with and without foundation, the latter predicting deflection of about 5.1 mm.

The shear responses (local responses) inside and outside the plastic hinge region as predicted by the three alternative analytical models are shown in Figure 14 (a) and 14 (b), respectively. Because of the restrained conditions and loading case, the plastic hinge is first formed at the midspan of frame (x=L/2) while the inelastic flexure deformation near the support (x=0) is not activated. Following the shear constitutive law, the shear response inside the plastic-hinge region shown in Figure 14 (a) is different from that outside the plastic-hinge region, shown in Figure 14 (b), due to the coupling effect between shear and flexure. It can be seen from Figure 14 (a) that the shear response from the proposed model starts to deviate from the undamaged primary curve to the damaged envelope curve when sectional curvature ductility demand is higher than 3, based on the UCSD shear-strength model within the framework of the shear-flexure interaction law. The sectional shear strain increases significantly until the failure is detected when the sectional shear strain reaches the ultimate $\gamma_u = 4.6x10^{-3}$. On the other hand, a series of the classical models follows the undamaged primary curve and cannot detect the shear failure at this section. Regarding the shear response outside the plastic-hinge region, shown in Figure 14 (b), it is clear from this plot that the shear responses from the three alternative analytical models are nearly identical and follow the undamaged primary curve. This relies on the fact that the inelastic flexural deformation (plastic-hinge formation) is not activated in this region. Finally, it is noted that the shear strain at the onset of the transverse reinforcement yielding γ_{st} in this simulation is equal to the shear strain at the onset of shear failure γ_u, predicted by Mergos and Kappos [36] in eq. (34).

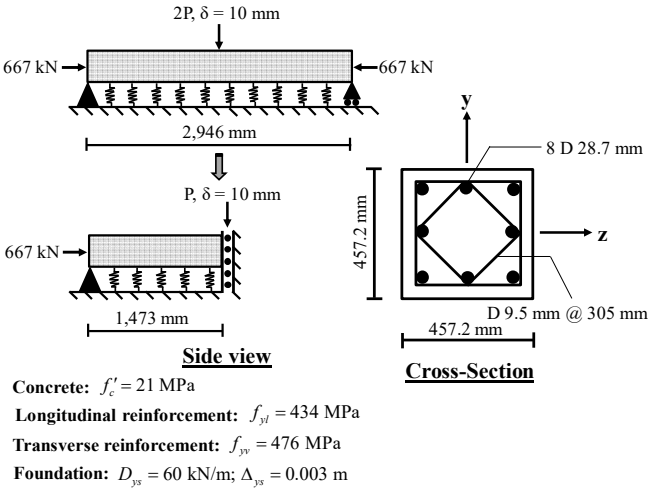

Fig. 10. Simulation I: Convergence studies.

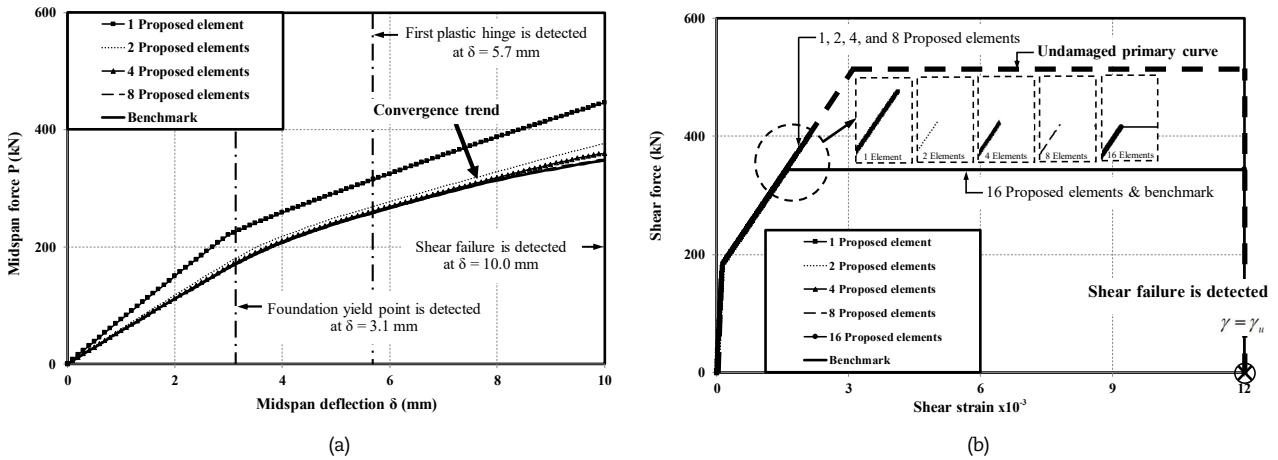

Fig. 11. Responses of Simulation I: (a) Global response; and (b) Local response.

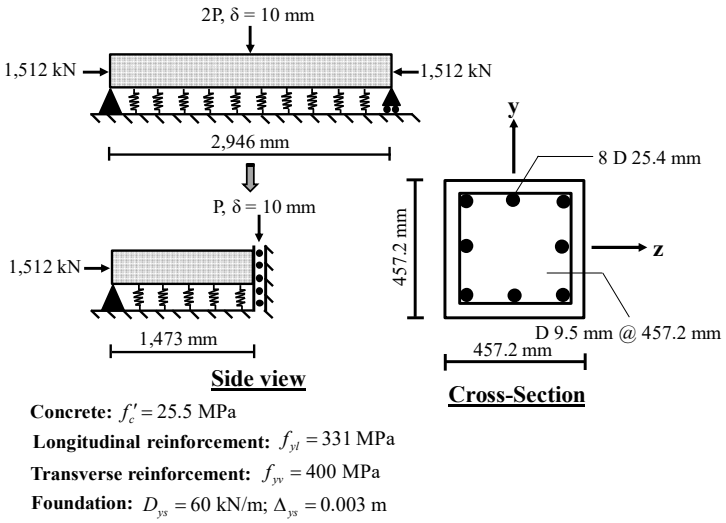

Fig. 12. Simulation II: RC frame on foundation.

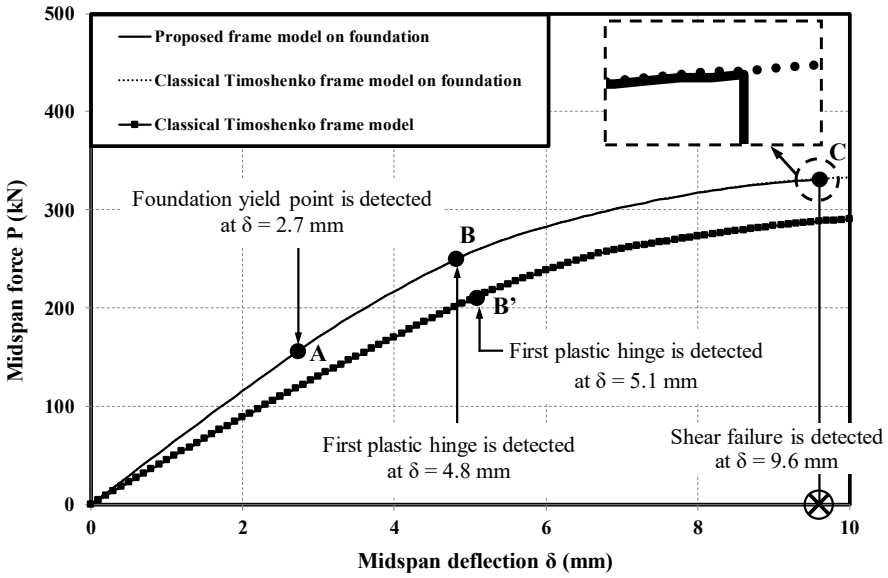

Fig. 13. Global response of simulation II.

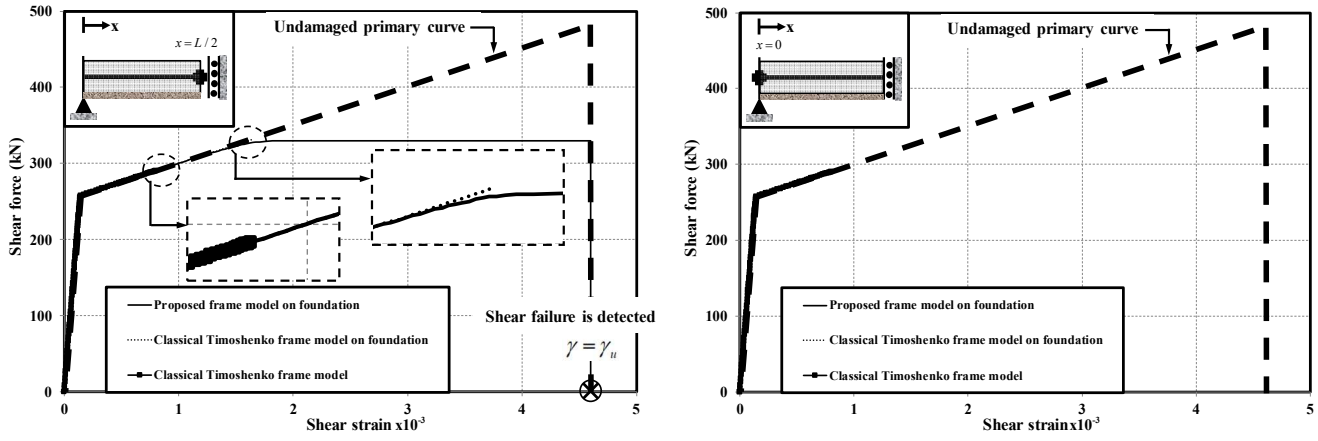

(a) (b)

Fig. 14. Shear response: (a) Inside the plastic hinge region at the midspan (x=L/2); and (b) Outside the plastic hinge region at the support (x=0).

Figure 15 presents the relation between shear force (demand) and the curvature ductility (demand) at the midspan of the frame member (x=L/2). The shear failure envelope (capacity) is established based on the UCSD shear-strength model with the initially predicted shear strength from eq. (33) of about $V_{u0} = 477.2\ kN$. It can be seen that the maximum shear force predicted by the proposed model of about $V_{max} = 329.8\ kN$ is less than the initial shear capacity. However, the peak shear force in this simulation occurs at the shear failure when the shear force demand meets the shear failure envelope (capacity) corresponding to curvature ductility demand of about $\mu_\varphi = 6.8$. This relies on the fact that if the shear and flexure actions had not interacted, this frame on foundation would not have failed in shear. On the other hand, a series of the classical models cannot detect this failure behavior due to the lack of consideration of the shear-flexure interaction effect, even if the shear force demand overlaps the shear failure envelope. Thus, the consideration of shear-flexure coupling effect within the model is absolutely necessary for investigations of non-ductile RC frame on foundation.

6. Conclusion

This paper presents a new fiber frame element on the Winkler-based foundation for the analysis of non-ductile reinforced concrete (RC) frames resting on foundation, which are flexure-shear critical members. A displacement-based finite element formulation was employed to formulate the proposed frame model based on the kinematics assumptions of Timoshenko beam theory. The nonlinear relations of the material models are represented (for uniaxial behavior) for concrete, reinforcing steel, shear response, and foundation. The shear-flexure interaction effect is taken into account in the proposed model in the framework of the UCSD shear-strength model. The inelastic flexural deformation (plastic-hinge formation) leads to reduced shear capacity, with degradation of sectional shear stiffness and shear force. The performance, efficiency, and ability of the proposed model were demonstrated by two simulations. The first simulation confirmed efficiency of the presented model through convergence studies of both global and local responses. Then, the second simulation confirmed importance of accounting for the shear-flexure interaction within the model for the analysis of non-ductile RC members resting on a foundation, when compared to the classical model. The proposed model can capture several salient features of the flexure-shear critical members on foundation, including the interaction effect between shear and flexural actions, the structure-soil interaction, the shear strength degradation associated with increasing curvature ductility demand, and the shear failure.

A step forward to develop the proposed frame element on the nonlinear foundation is extending the model to cover both two-parameter and three-parameter foundations for the nonlinear analysis of non-ductile RC frame structures on the foundation, with interaction effect between shear and flexural mechanisms. Therefore, the developed shear-flexure-based frame element on the foundation may play an essential role further studies of structural engineering.

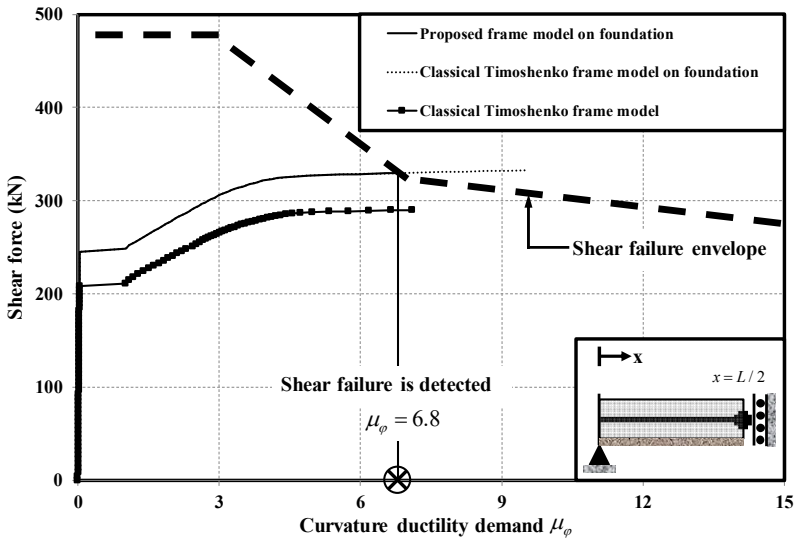

Fig. 15. Shear demand vs shear capacity inside the plastic hinge region at the midspan (x=L/2).

Author Contributions

Worathep Sae-Long plays a role in implementing the numerical model, interpreting the numerical results, and partially writing the manuscript; Suchart Limkatanyu plays a role in formulating the numerical model, interpreting the numerical results and partially writing the manuscript; Pattamad Panedpojaman and Woraphot Prachasaree plays a role in revising the manuscript; Nattapong Damrongwiriyanupap and Minho Kwon plays a role in discussing the numerical results and partially writing the manuscript; and Chayanon Hansapinyo plays a role in interpreting the numerical results. The manuscript was written through the contribution of all authors. All authors discussed the results, reviewed and approved the final version of the manuscript.

Acknowledgments

Financial support of this work was provided by the Thailand Research Fund (TRF) under Grant RTA6280012 and by the National Research Foundation of Korea (NRF) funded by the Government of South Korea (Ministry of Science and ICT; MSIT) (No.2019R1A2C1003007). Furthermore, we would like to sincerely thank the copy-editing service of Research and Development Office, and Assoc. Prof. Dr. Seppo Karrila who dedicated his time to provide valuable comments, and gratefully acknowledge the support and assistance received.

Conflict of Interest

The authors declared no potential conflicts of interest with respect to the research, authorship and publication of this article.

Funding

Financial support of this work was provided by the Thailand Research Fund (TRF) under Grant RTA6280012 and by the National Research Foundation of Korea (NRF) funded by the Government of South Korea (Ministry of Science and ICT; MSIT) (No.2019R1A2C1003007).

References

[1] Alisjahbana, S.W., Alisjahabana, I., Kiryu, S., Gan, B.S., Semi analytical solution of a rigid pavement under a moving load on a Kerr foundation model, *Journal of Vibroengineering*, 20(5), 2018, 2165-2174.
[2] Heymsfield, E., Tingle, J.S., State of the practice in pavement structural design/analysis codes relevant to airfield pavement design, *Engineering Failure Analysis*, 105, 2019, 12-24.
[3] Chen, X.L., Yang, Q.H., Ding, J.P., Mechanical characterization of beams on tensionless foundation materials, *Materials Science Forum*, 867, 2016, 152-156.
[4] Rahman, Md.S., Hasan, A.S., Yeasmin, I.A., Modified multi-level residue harmonic balance method for solving nonlinear vibration problem of beam resting on nonlinear elastic foundation, *Journal of Applied and Computational Mechanics*, 5(4), 2019, 627-638.
[5] Limkatanyu, S., Kwon, M., Prachasaree, W., Chaiviriyawong, P., Contact interface fiber section element: shallow foundation modeling, *Geomechanics and Engineering*, 4(3), 2012, 173-190.
[6] Limkatanyu, S., Kuntiyawichai, K., Spacone, E., Kwon, M., Natural stiffness matrix for beams on Winkler foundation: Exact force-based derivation, *Structural Engineering and Mechanics*, 42(1), 2012, 39-53.
[7] Saadatinezhad, M., Lakirouhani, A., Jabini Asli, S., Seismic response of non-connected piled raft foundations, *International Journal of Geotechnical Engineering*, 2019, 1-15.
[8] Dutta, S.C., Roy, R., A critical review on idealization and modeling for interaction among soil-foundation-structure system, *Computers & Structures*, 80(20-21), 2002, 1579-1594.
[9] Menglin, L., Huaifeng, W., Xi, C., Yongmei, Z., Structure-soil-structure interaction: Literature review, *Soil Dynamics and Earthquake Engineering*, 31(12), 2011, 1724-1731.
[10] Boussinesq, H., *Applications des Potentiels al'Etude de l'Equilibre et du Mouvement des Solids Elastique*, Gauthier-Villars, Paris, 1885.
[11] Foppl, A., *Vorlesungen über Technische Mechanik*, B. B. Teubner, Leipzig, 1909.
[12] Selvadurai, A.P.S., *Elastic analysis of soil-foundation interaction*, Elsevier Publishing Company, Inc., NewYork, 1979.
[13] Winkler, E., *Die lehre von der elastizität und Festigkeit*, Prag, 1867.
[14] Timoshenko, S.P., Gere, J.M., *Theory of elastic stability engineering societies monographs*, McGraw-Hill Book Company, New York, 1961.
[15] Cheng, F.Y., Pantelides, C.P., Dynamic Timoshenko beam-column on elastic media, *Journal of Structural Engineering*, 114(7), 1988, 1524-1550.
[16] Monsalve, A.L.G., Medina, Z.D.G., Ochoa, A.J.D., Timoshenko beam-column with generalized end conditions on elastic foundation: Dynamic-stiffness matrix and load vector, *Journal of Sound and Vibration*, 310(4-5), 2008, 1057-1079.
[17] Yokoyama, T., Vibration analysis of Timoshenko beam-columns on two-parameter elastic foundations, *Computers & Structures*, 61(6), 1996, 995-1007.
[18] Taha, M.H., Abdeen, M.A.M., Analytical solutions for Timoshenko beam-columns on elastic foundations, *Arabian Journal for Science and Engineering*, 41(10), 2016, 4053-4064.
[19] Ghee, A., Priestley, M.J.N., Paulay, T., Seismic shear strength of circular reinforced concrete columns, *ACI Structural Journal*, 86(1), 1989, 45-59.
[20] Priestley, M.J.N., Seible, F., Verma, R., Xiao, Y., Seismic shear strength of reinforced concrete columns, *Structural Systems Research Project Report No. SSRP 93/06*, University of California, San Diego, USA, 1993.
[21] Li, X., Reinforced concrete columns under seismic lateral force and varying axial load, Ph.D. Thesis, Department of Civil Engineering, University of Canterbury, Christchurch, New Zealand, 1994.
[22] Lynn, A.C., Seismic evaluation of existing reinforced concrete building columns, Ph.D. Thesis, Department of Civil and Environmental Engineering, University of California, Berkeley, USA, 2001.
[23] Sezen, H., Seismic behavior and modeling of reinforced concrete building columns, Ph.D. Thesis, Department of Civil and Environmental Engineering, University of California, Berkeley, USA, 2002.
[24] Sezen, H., Moehle, J.P., Shear strength model for lightly reinforced concrete columns, *Journal of Structural Engineering*, 130(11), 2004, 1692-1703.
[25] Ceresa, P., Petrini, L., Pinho, R., Flexure-shear fiber beam-column elements for modeling frame structures under seismic loading: State of the art, *Journal of Earthquake Engineering*, 11(supplement 1), 2007, 46-88.
[26] Petrangeli, M., Pinto, P.E., Ciampi, V., Fiber element for cyclic bending and shear of RC structures. I: Theory, *Journal of Engineering Mechanics*, 125(9), 1999, 994-1001.
[27] Stramandinoli, R.S.B., Rovere, H.L.L., FE model for nonlinear analysis of reinforced concrete beams considering shear deformation, *Engineering Structures*, 35, 2012, 244-253.
[28] Long, X., Bao, J.Q., Tan, K.H., Lee, C.K., Numerical simulation of reinforced concrete beam/column failure considering normal-shear stress interaction, *Engineering Structures*, 74, 2014, 32-43.
[29] Li, Z.X., Gao, Y., Zhao, Q., A 3D flexure-shear fiber element for modeling the seismic behavior of reinforced concrete columns, *Engineering Structures*, 117, 2016, 372-383.
[30] Feng, D.C., Wu, G., Sun, Z.Y., Xu, J.G., A flexure-shear Timoshenko fiber beam element based on softened damage-plasticity model, *Engineering Structures*, 140, 2017, 483-497.
[31] Marini, A., Spacone, E., Analysis of reinforced concrete elements including shear effects, *ACI Structural Journal*, 103(5), 2006, 645-655.
[32] Eurocode No. 2: Design of concrete structures-part 1-1: General rules and rules for buildings. ENV 1992-1-1, Brusse, 1991.
[33] Mergos, P.E., Kappos, A.J., A distributed shear and flexural flexibility model with shear-flexure interaction for R/C members subjected to seismic loading, *Earthquake Engineering & Structural Dynamics*, 37(12), 2008, 1349-1370.
[34] Soleimani, D., Reinforced concrete ductile frames under earthquake loadings with stiffness degradation, Ph.D. Thesis, University of California, Berkeley, USA, 1978.
[35] Ozcebe, G., Saatcioglu, M., Hysteretic shear model for reinforced concrete members, *Journal of Structural Engineering*, 115(1), 1989, 132-148.
[36] Mergos, P.E., Kappos, A.J., A gradual spread inelasticity model for R/C beam-columns, accounting for flexure, shear and anchorage slip, *Engineering Structures*, 44, 2012, 94-106.
[37] Zimos, D.K., Mergos, P.E., Kappos, A.J., Modelling of R/C members accounting for shear failure localisation: Hysteretic shear model, *Earthquake Engineering & Structural Dynamics*, 47(7), 2018, 1631-1650.
[38] Xu, S.Y., Zhang, J., Hysteretic shear–flexure interaction model of reinforced concrete columns for seismic response assessment of bridges, *Earthquake Engineering & Structural Dynamics*, 40(3), 2011, 315-337.
[39] Sae-Long, W., Limkatanyu, S., Prachasaree, W., Horpibulsuk, S., Panedpojaman, P., Nonlinear frame element with shear-flexure interaction for seismic analysis of non-ductile reinforced concrete columns, *International Journal of Concrete Structures and Materials*, 13, 2019, Article number: 32.
[40] Sae-Long, W., Limkatanyu, S., Hansapinyo, C., Imjai, T., Kwon, M., Forced-based shear-flexure-interaction frame element for nonlinear analysis of non-ductile reinforced concrete columns, *Journal of Applied and Computational Mechanics*, (2021) (In press).
[41] Tonti, E., The reason for analogies between physical theories, *Applied Mathematical Modelling*, 1(1), 1976, 37-50.
[42] Taylor, R.L., *FEAP: A finite element analysis program*, User manual: version 7.3, Department of Civil and Environmental Engineering, University of California, Berkeley, USA, 2000.
[43] Onate, E., *Structural analysis with the finite element method volume 2: beams, plates and shells*, Springer, Netherlands, 2013.

[44] Limkatanyu, S., Kuntiyawichai, K., Spacone, E., Kwon, M., Nonlinear Winkler-based beam element with improved displacement shape functions, *KSCE Journal of Civil Engineering*, 17(1), 2013, 192-201.
[45] Spacone, E., Limkatanyu, S., Responses of reinforced concrete members including bond-slip effects, *ACI Structural Journal*, 97(6), 2000, 831-839.
[46] Kent, D.C., Park, R., Flexural members with confined concrete, *Journal of the Structural Division*, 97(7), 1971, 1964-1990.
[47] Menegotto, M., Pinto, P.E., Method of analysis for cyclically loaded reinforced concrete plane frames including changes in geometry and nonelastic behavior of elements under combined normal force and bending, *Proceeding of IABSE Symposium on Resistance and Ultimate Deformability of Structures Acted on by Well-Defined Repeated Loads*, Lisbon, 1973, 15-22.
[48] Fraeijs de Veubeke, B.M., *Displacement and equilibrium models*, Chapter 9 in Stress Analysis, Wiley, London, 1965, 145-197.
[49] Sezen, H., Moehle, J.P., Shear strength model for lightly reinforced concrete column, *Journal of Structural Engineering*, 130(11), 2004, 1692-1703.
[50] Park, R., Paulay, T., *Reinforced concrete structures*, John Wiley & Sons, New York, 1975.
[51] Ma, S.M., Bertero, V.V., Popov, E.P., Experimental and analytical studies on hysteretic behavior of RC rectangular and T-beam, *Earthquake Engineering Research Center Report No. UCB/EERC-76/02*, University of California, Berkeley, USA, 1976.
[52] Aboutaha, R.S., Engelhardt, M.D., Jirsa, J.O., Kreger, M.E., Rehabilitation of shear critical concrete columns by use of rectangular steel jackets, *ACI Structural Journal*, 96(1), 1999, 68-78.
[53] Gerin, M., Adebar, P., Accounting for shear in seismic analysis of concrete structures. *Proceeding of 13th world conference on earthquake engineering*, Vancouver, B.C., Canada, Paper No. 1747, 2004.
[54] Sezen, H., Shear deformation model for reinforced concrete columns, *Structural Engineering and Mechanics*, 28(1), 2008, 39-52.
[55] Watanabe, F., Ichinose, T., Strength and ductility design of RC members subjected to combined bending and shear, *Proceeding of workshop on concrete shear in earthquake*, University of Houston, Texas, 1991, 429-438.
[56] Chapra, S.C., Canale, R.P., *Numerical methods for engineers*, McGraw-Hill, New York, 2002.
[57] Biskinis, D., Roupakias, G., Fardis, M., Degradation of shear strength of reinforced concrete members with inelastic cyclic displacement, *ACI Structural Journal*, 101(6), 2004, 773-783.
[58] Sapountzakis, E.J., Kampitsis, A.E., Inelastic analysis of beams on two-parameter tensionless elastoplastic foundation, *Engineering Structures*, 48, 2013, 389-401.

ORCID iD

Worathep Sae-Long https://orcid.org/0000-0001-8149-4409
Suchart Limkatanyu https://orcid.org/0000-0002-4343-7654
Woraphot Prachasaree https://orcid.org/0000-0002-0447-4997
Nattapong Damrongwiriyanupap https://orcid.org/0000-0001-7280-5957
Minho Kwon https://orcid.org/0000-0003-0754-285X
Chayanon Hansapinyo https://orcid.org/0000-0002-6237-613X

How to cite this article: Sae-Long W. *et al*. Nonlinear Winkler-based Frame Element with Inclusion of Shear-Flexure Interaction Effect for Analysis of Non-Ductile RC Members on Foundation, *J. Appl. Comput. Mech.*, 7(1), 2021, 148–164.
https://doi.org/10.22055/JACM.2020.34699.2460